IN SITU VISUALIZATION OF FLOW AND FOULING LAYER FORMATION IN CERAMIC HOLLOW FIBER MEMBRANES BY MAGNETIC RESONANCE IMAGING (MRI)

Felicitas Arndt[1]*, Sebastian Schuhmann[1], Gisela Guthausen[1], Steffen Schütz[2], Hermann Nirschl[1]

[1]MVM, Karlsruhe Institute of Technology (KIT)

[2]MANN+HUMMEL GmbH, Ludwigsburg

ABSTRACT

Within membrane processes, fouling is one of the critical issues affecting the productivity, plant operation and maintenance costs. Focusing on wastewater treatment processes, it has been reported that extracellular polymeric substances (EPS) are one of the main causes of membrane fouling. In membrane filtration research, sodium alginate often serves as a model compound for EPS. Sodium alginate is a hydrophilic unbranched binary copolymer. In the presence of divalent cations, e.g. Ca^{2+}, alginates form complexes, which lead to a significant change in filtration mechanisms in dead-end filtration and also to a change in filtration performance during cross-flow filtration experiments. Filtration conditions (e.g. transmembrane pressure or cross flow velocity), feed composition as well as membrane material have a major influence on the fouling behavior of the system. In this study ceramic hollow fiber membranes were used due to their high chemical and thermal stability coupled with a high specific membrane surface.

In addition to the evaluation of the filtration data using conventional cake filtration model, nuclear magnetic resonance imaging was used to elucidate the influence of Ca^{2+} on the fouling layer structure for alginate filtration with ceramic hollow fiber membranes. In order to visualize the alginate layers inside the opaque ceramic hollow fiber membranes by means of MRI, specific contrast agents were applied. Supplementary to multi slice multi echo imaging, flow velocity measurements were performed to gain more insight into the hydrodynamics in the fouled membranes.

MRI reveals the structure of the alginate layers and confirms the assumption obtained from the evaluation of filtration data, that the addition of Ca^{2+} is leading to the formation of an alginate gel layer on the membrane, whereas in the absence of Ca^{2+}, the structure of the alginate layer is rather of concentration polarization manner, hence more fluid and hydrodynamically better controllable.

KEYWORDS

MRI, ceramic membrane, hollow fiber, alginate

1 Introduction

Membrane fouling is one of the critical issues affecting the productivity, plant operation and maintenance costs in membrane filtration [1]. For the description of membrane fouling mechanisms, different models can be applied, e.g. resistance in series analysis can be performed [2]. Despite of the fact that these models enable to study fouling phenomena systematically, they have one major drawback. The resulting filtration data is commonly spatially averaged over the whole membrane module. These techniques provide no insight into local fouling phenomena which might change along the membrane's long axis due to local variations of the transmembrane pressure (TMP) or axial dependency of the flux or permeate along the hollow fiber module [3]. Therefore it would be desirable to use complementary characterisation techniques to gain more insight into these spatially varying fouling phenomena. Nuclear magnetic resonance (NMR) imaging is known to be a powerful technique for non-invasive observation of membrane processes [4-6]. In our study we focus on sodium alginate as model substance. Sodium alginate is often used in membrane filtration research as a model compound for extracellular polymeric substance, which are discussed as major foulants in waste water treatment processes [2, 7-11]. Sodium alginate is a negatively charged polysaccharide and very sensitive to changes in ionic strength. Alginates form aggregates in presence of divalent cations, such as Ca^{2+}. The Ca^{2+} binds preferentially to the carboxylic groups of alginates, leading to a highly organized network which can be illustrated by the "egg-box" model [2, 7]. MRI in material science often uses relaxation differences to visualize structures in heterogeneous samples. In the context MRI on filtration processes, the feed often contains particles with their inherent small transverse relaxation times leading to a negative image contrast. In the case of alginate filtration, both the relaxation times of water and alginate solution are rather similar. The same is valid for diffusion properties, leading to a vanishing image contrast. Therefore, contrast agents were applied.

2 Experimental

2.1 Materials

2.1.1 Ceramic Hollow Fibers Membranes

The investigated ceramic hollow fiber membranes with an inner diameter around 1.8 mm consist of two layers: a supportive layer and a thin active layer of Al_2O_3, located at the inner side of the membrane (Fig. 1). The membranes are characterized by high chemical and thermal stability as well as a high specific membrane filter surface.

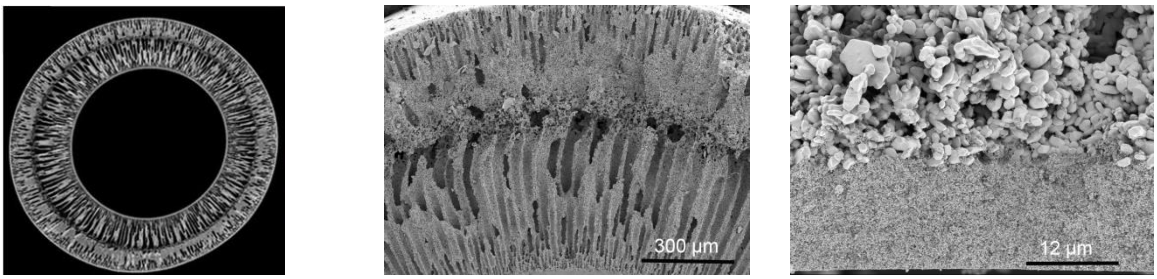

Figure 1 µCT and SEM images of a ceramic hollow fiber membrane. Left: µCT image of a hollow fiber membrane illustrates the open pore structure of the support layer. Middle: Detail of the cross section of the hollow fiber membrane showing the porous support layer. Right: Detail of the active layer on the inside the hollow fiber membrane and transition to the support layer [12].

2.1.2 Feed solution

Sodium alginate ("medium viscosity") from brown algae with a reported molecular weight of 80-120 kDa was purchased from Sigma Aldrich. For each experiment fresh stock solutions of 1 g/l sodium alginate were prepared in ultrapure water. The feed solutions with a pH value of 6.2 were subsequently prepared by dilution of the stock solution with the proper amount of ultrapure water to adjust the desired concentration. The sodium alginate concentration in this study was 200 mg/l except where otherwise noted. For experiments with calcium ions, $CaCl_2$ was added out of a 2 g/l stock solution to the feed solution prior the filtration step in order to prevent overdosing.

2.1.3 Contrast Agent MION

Specific alginate coated Magnetic iron oxide nanocrystallites (MIONs) were applied as contrast agents. The MIONS reduce the relaxation times of molecules in their neighbourhood via paramagnetic relaxation enhancement (PRE), which leads to a negative contrast for the chosen MRI parameters. The effect of contrast agent addition is shown in Fig. 2.

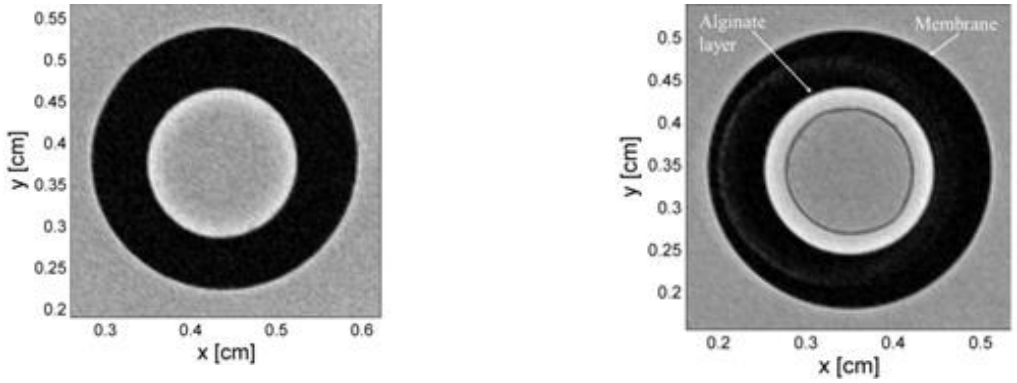

Figure 2 Influence of the contrast agent on the localizability of the alginate layer. Left: Membrane after dead-end filtration of 200 mg/l alginate with addition of 2 mmol/l Ca^{2+} without addition of MIONs and right: after addition of MIONs [12].

The left image of figure 2 is obtained after dead-end filtration of 200 mg/l alginate with addition of 2 mmol/l Ca^{2+}. In the images the membrane appears black, the water inside and outside creates the contrast. The bright area on the inner surface of the hollow fiber could be attributed to a higher concentration of alginate, but the structure could not be quantified. When adding 100 µl contrast agent MagAlgPEG (c_{Fe} = 0,52 mM) the image changes: The MIONs accumulate at the surface of the alginate gel layer. As the PRE is always concentration dependent and as the concentration of the MIONs varies with position due to agglomeration, a specific contrast in the image was generated. As a result the structure of the gel layer can be visualized.

2.2 Experimental set-up

MRI filtration experiments have been performed with a single fiber module in an *in-situ* filtration set-up. The filtration module is mounted into a Bruker 200 MHz SWB magnet for MRI. The feed is filtered from the inside to the outside of the membrane, leading to a fouling layer at the inner surface of the cylindrical hollow fiber membrane. The desired cross-flow velocity can be regulated by the throttle valve in the retentate line. In dead-end experiments, the throttle valve is closed whereas it is open in cross-flow filtration. A pressure vessel is used as feed source in order to minimize pulsations, because this would lead to artefacts in the images.

The fouling layer build up was measured time-resolved for dead-end filtrations at 100 kPa of two different feed solutions (200 mg/l sodium alginate without and with addition of 2 mmol/l Ca^{2+}), the MIONs are added directly in the feed solution. The permeate flux was measured simultaneously to obtain the classical characterizing parameters of filtration. The combination of both, the classical way and the quantification of the fouling layer by MRI image analysis result in a more detailed insight into the filtration process. The fouling layer thickness correlates with the permeate flux.

3 Results and Discussion

3.1 Fouling layer structure

Figure 3 displays the fouling layer structure for alginate dead-end filtrations with and without Ca^{2+} added to the feed solution. Due to the addition of MIONs directly to the feed solution the alginate layer exhibits a negative contrast. With Ca^{2+} the fouling layer is compact and relatively thin, indicating the formation of a structured gel layer. Without Ca^{2+} addition an unstructured, irregular layer develops with increasing filtration time.

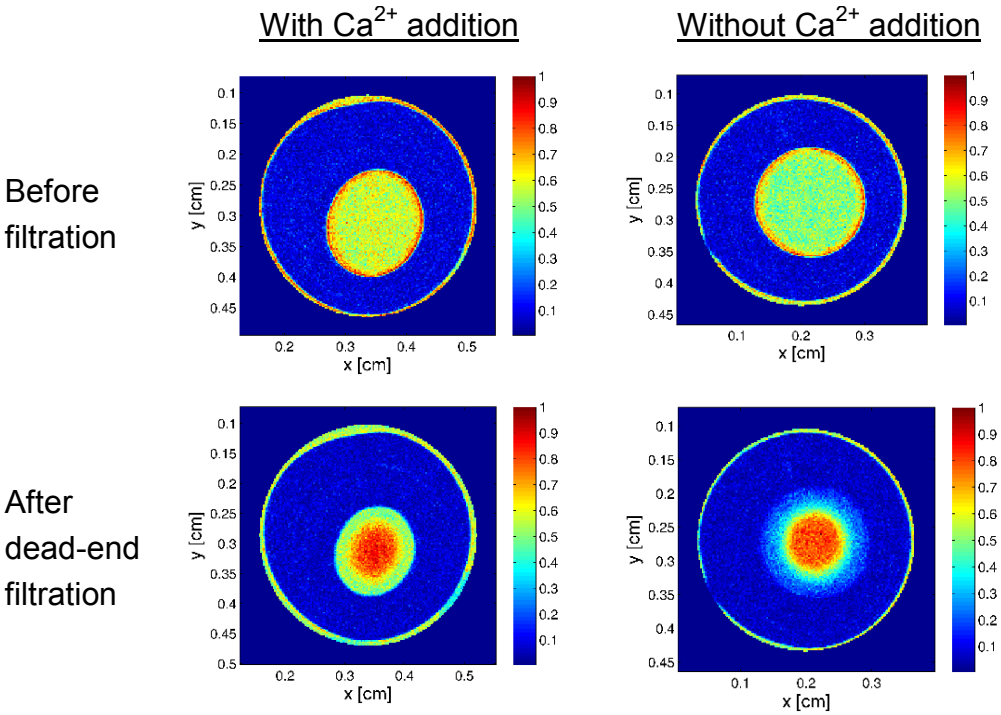

Figure 3: Alginate dead-end filtration with and without Ca^{2+} as observed in RARE images.

In the dead-end mode the medium being filtrated is pressed completely through the membrane leading to a growth of the resulting fouling layer causing rapid permeability decay. Permeate flux can be calculated using Darcy´s law for constant pressure filtration:

$$J = \frac{\Delta P}{\eta\,(R_{Ges})} \qquad (1)$$

J is permeate flux, ΔP is transmembrane pressure, η is dynamic viscosity and R_{Ges} is total resistance consisting of the membrane hydraulic resistance and different resistances caused by fouling (e.g. internal pore blocking or cake formation)[13]. These fouling mechanisms can be analyzed by plotting the flux data in an appropriate linearized form according to the following model:

$$\frac{t}{V} = \frac{\eta R_m}{\Delta P \cdot A} + \left(\frac{\eta \alpha c_b}{2\Delta P \cdot A^2}\right) V \qquad (2)$$

R_m is membrane hydraulic resistance, A is active filtration area of the membrane, V is filtrate volume, α is specific cake resistance and c_b is bulk concentration of organic foulant (e.g. alginate). A straight line as result of this kind of replotting t/V = f(V) means cake formation is the only fouling mechanism taking place. Figure 4 displays the filtration data of dead-end filtrations in presence and absence of Ca^{2+} and the corresponding fouling layer heights, obtained by evaluation of the MRI images.

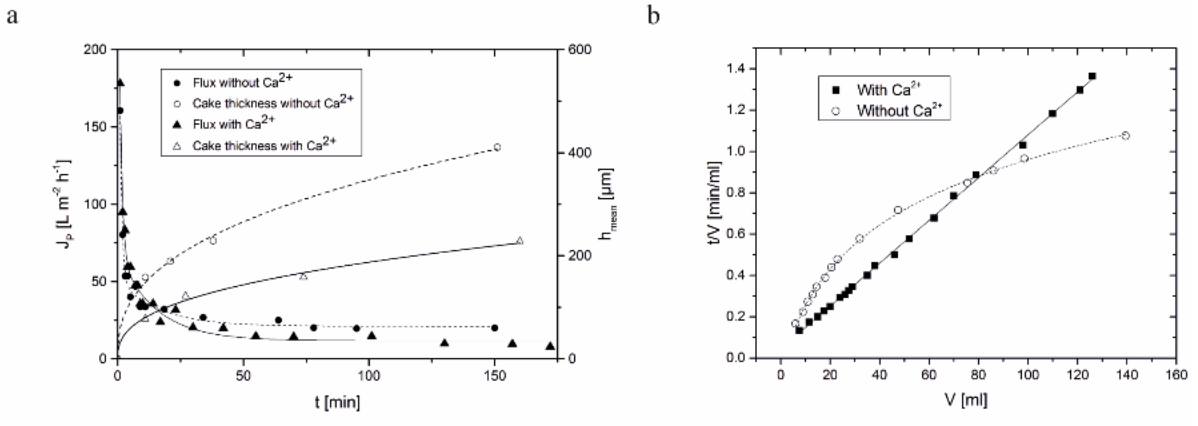

Figure 4: a) Permeate flux J_P from filtration experiments and fouling layer thickness h_m from *in-situ* MRI as a function of filtration time for a dead-end filtration at 100 kPa. Both measurements reflect the filtration mechanisms of alginate filtration with and without Ca^{2+}, which can be described by replotting the filtration data according to the filtration model in a t/V divided by V diagram shown in b). Filtration mechanisms change from pore blocking followed by cake filtration (without Ca^{2+}) to cake filtration only (with Ca^{2+}) (V >60 ml).

The thickness of the fouling layer rapidly increases at the beginning of the dead-end filtration experiment in presence and in absence of Ca^{2+} (Figure 4a, $t \in [0, 25]$ min). In this period, the permeate flux also decreases rapidly. After this initial phase, the permeate fluxes are nearly constant, while J_P for filtration of alginate solutions without Ca^{2+} is slightly higher compared to J_P with Ca^{2+} addition. On the other hand, the fouling layer for alginate filtration with Ca^{2+} is significantly thinner than in the case of alginate filtration without Ca^{2+}. On a first look, this seems to be contradictory to the lower flux in case of Ca^{2+} alginate filtration, but on a closer look, the fouling layer in absence of Ca^{2+} has a lower density and is better described by loose or fluffy structures. It therefore has a significantly lower resistance than the compact layer observed in presence of Ca^{2+}. This finding is also obvious in the classical t/V versus t diagram which is used for characterization of filtration mechanisms: In the case of alginate filtration with Ca^{2+}, the filtration process can be described as cake filtration, where typically a linear relation between t/V and V is observed. The filtration without

Ca^{2+} is, due to the higher slope at the beginning of the filtration, better described by pore blocking in the early filtration stage followed by cake filtration mechanism. The much lower slope in this filtration stage is also related with the less dense structure of the alginate layer, indicating the formation of concentration polarization layer and not a dense gel layer for the filtration of alginate without Ca^{2+}. These findings are discussed deeper in the following section.

3.2 Time dependence of flow velocities during dead-end filtration

Not only the structure of the fouling layer is influenced by the presence or absence of Ca^{2+}, also the flow velocity profiles are different. They were investigated and analyzed especially inside the feed channel of the membrane. Alginate solutions ($c_{Alginate}$ = 200 mg/l) with c_{Ca2+} = 2 mmol/l and c_{Ca2+} = 0 mmol/l were filtered under the same dead-end filtration conditions as previously noted (TMP = 100 kPa). The MSME pulse sequence was applied to visualize flow profiles by saturation stripes, thus to measure 2D spatially resolved flow velocity profiles $v_z(r)$ in the center of the membrane.

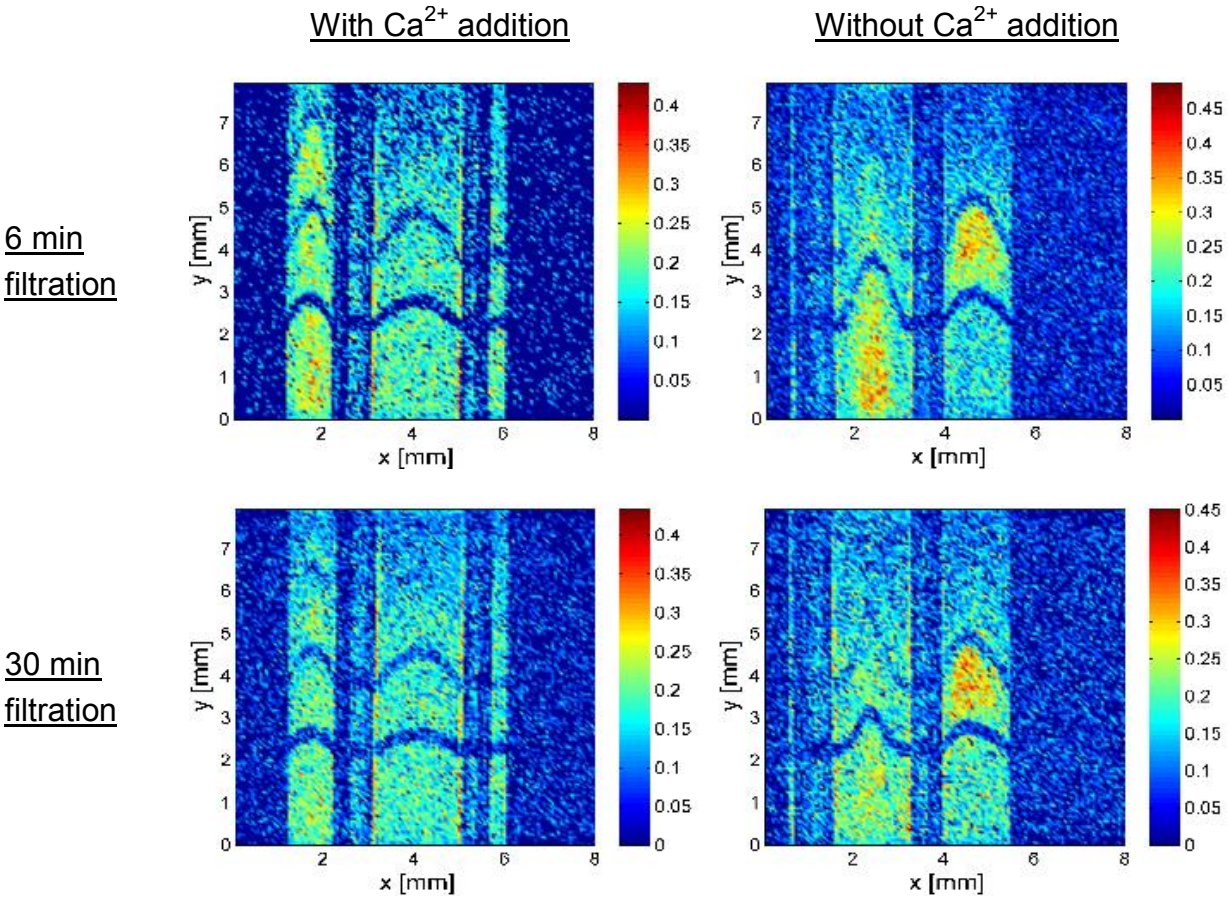

Figure 5: Saturation stripes indicate displacements, i.e. $v_z(r)$ in and outside of the membrane. Left: *In-situ* dead-end filtration with Ca^{2+} at filtration times of 3 and 30 min. right: *In-situ* dead-end filtration without Ca^{2+} addition at filtration times of 3 and 30 min. The form of the saturation stripes, i.e. of the flow profiles depends clearly on the Ca^{2+} concentration.

As expected, flow velocity decreases with progressing filtration in both cases without and with Ca^{2+}. For filtration conditions in presence of Ca^{2+} the form corresponds to the expectations of approximately tubular flow: As the permeate flow rate is rather low in the measured part of the fiber, the flow profile in the cylindrical hollow is describable by a tube flow in a good approximation. Hardly a change in the flow profile shape is observed as a function of filtration time. For filtration without Ca^{2+} the observation is different. A change in the shape of the saturation stripes occurs. With progressing filtration duration, it deviates clearly and increasingly from the signature of tubular flow. This change in shape of the flow profile might be initiated by the large concentration polarization layer in absence of Ca^{2+}. Due to the increase of the alginate concentration in direction of the membrane wall, also the viscosity increases. This leads to a deviation of the flow profile from expected Hagen-Poiseuille flow. In presence of Ca^{2+} the molecules are bound in the alginate gel layer, the back diffusion and therefore the build-up of a large concentration polarization layer is restricted and the viscosity remains more constant in the cross section of the membrane lumen.

Literature

[1] P. Le-Clech, V. Chen, T.A.G. Fane, Fouling in membrane bioreactors used in wastewater treatment, Journal of Membrane Science, 284 (2006) 17-53.
[2] K. Listiarini, W. Chun, D.D. Sun, J.O. Leckie, Fouling mechanism and resistance analyses of systems containing sodium alginate, calcium, alum and their combination in dead-end fouling of nanofiltration membranes, Journal of Membrane Science, 344 (2009) 244-251.
[3] W.J.C. van de Ven, K.v.t. Sant, I.G.M. Pünt, A. Zwijnenburg, A.J.B. Kemperman, W.G.J. van der Meer, M. Wessling, Hollow fiber dead-end ultrafiltration: Influence of ionic environment on filtration of alginates, Journal of Membrane Science, 308 (2008) 218-229.
[4] S. Bütehorn, Experimental and Numerical Investigation of the Hydrodynamics of Microfiltration Processes Using a Multi-Scale Approach in, Rheinisch-Westfälischen Technischen Hochschule Aachen, Aachen, 2011.
[5] J.C. Chen, Q. Li, M. Elimelech, In situ monitoring techniques for concentration polarization and fouling phenomena in membrane filtration, Advances in Colloid and Interface Science, 107 (2004) 83-108.
[6] V. Chen, H. Li, A.G. Fane, Non-invasive observation of synthetic membrane processes – a review of methods, Journal of Membrane Science, 241 (2004) 23-44.
[7] K. Katsoufidou, S.G. Yiantsios, A.J. Karabelas, Experimental study of ultrafiltration membrane fouling by sodium alginate and flux recovery by backwashing, Journal of Membrane Science, 300 (2007) 137-146.
[8] Y. Ye, P. Le Clech, V. Chen, A.G. Fane, B. Jefferson, Fouling mechanisms of alginate solutions as model extracellular polymeric substances, Desalination, 175 (2005) 7-20.
[9] K. Katsoufidou, S.G. Yiantsios, A.J. Karabelas, An experimental study of UF membrane fouling by humic acid and sodium alginate solutions: the effect of backwashing on flux recovery, Desalination, 220 (2008) 214-227.
[10] M. Hashino, T. Katagiri, N. Kubota, Y. Ohmukai, T. Maruyama, H. Matsuyama, Effect of membrane surface morphology on membrane fouling with sodium alginate, Journal of Membrane Science, 366 (2011) 258-265.
[11] Y. Ye, V. Chen, A.G. Fane, Modeling long-term subcritical filtration of model EPS solutions, Desalination, 191 (2006) 318-327.
[12] F. Arndt, U. Roth, H. Nirschl, S. Schütz, G. Guthausen, New insights into sodium alginate fouling of ceramic hollow fiber membranes by NMR imaging, AIChE Journal, 62 (2016) 2459-2467.
[13] K. Listiarini, W. Chun, D.D. Sun, J.O. Leckie, Fouling mechanism and resistance analyses of systems containing sodium alginate, calcium, alum and their combination in dead-end fouling of nanofiltration membranes, in: Journal of Membrane Science 344, 2009, pp. 244-251.